

# Polymerization Force Driven Buckling of Microtubule Bundles Determines the Wavelength of Patterns Formed in Tubulin Solutions

Yongxing Guo, Yifeng Liu, Jay X. Tang, and James M. Valles, Jr.  
 Physics Department, Brown University, Providence, RI 02912  
 (Dated: June 8, 2021)

We present a model for the spontaneous formation of a striated pattern in polymerizing microtubule solutions. It describes the buckling of a single microtubule (MT) bundle within an elastic network formed by other similarly aligned and buckling bundles and unaligned MTs. Phase contrast and polarization microscopy studies of the temporal evolution of the pattern imply that the polymerization of MTs within the bundles creates the driving compressional force. Using the measured rate of buckling, the established MT force-velocity curve and the pattern wavelength, we obtain reasonable estimates for the MT bundle bending rigidity and the elastic constant of the network. The analysis implies that the bundles buckle as solid rods.

Microtubules (MTs), a major component of the eukaryotic cytoskeleton [1], can form various structures and patterns. For example, *in vivo*, MTs organize into the spindles and asters essential for mitosis [2] and the parallel arrays and stripes necessary for directing early processes in embryogenesis [3, 4]. Many *in vitro* studies of MT organization have been performed in order to elucidate the mechanisms underlying the formation of these structures [5, 6, 7, 8]. Of particular relevance here are the striped birefringent patterns [Fig. 1(a)], which spontaneously form from polymerizing a purified tubulin solution without motor proteins or MT associated proteins. Hitt *et al.* attributed these patterns to the formation of nematic liquid crystalline domains [5]. Tabony *et al.*, on the other hand, proposed that a reaction-diffusion based mechanism drives the formation of MT stripes [6]. Our recent investigations imply a starkly different scenario in which the local MT alignment into wave-like structures occurs through a collective process of MT bundling and buckling [9]. MTs that are aligned by a static magnetic field [10, 11] or convective flow [9] during the initial stage of polymerization spontaneously form bundles in tubulin solutions with concentrations of a few mg/ml. These bundles elongate and buckle in coordination with neighboring bundles into a wave-like shape. The nesting of the buckled bundles can quantitatively account for the MT density and orientation variations leading to the striped birefringent pattern [9]. We proposed that a compressional force is generated by MT polymerization occurring uniformly along the bundle contours. The buckling wavelength is controlled by the bending rigidity of the bundles and the elasticity of the background network of MTs. This interesting initial assessment calls for further investigation of the microscopic picture of the bundle elongation, the MT buckling force and the buckling mode selection mechanism.

Here we present a mechanical model for the process in addition to new experimental data on the time evolution of the bundle contour length and solution birefringence that provide direct support for the validity of the model. The model considers the instability of a single MT bundle under a compressional force, embedded in an elastic network formed by both bundled and dispersed MTs. Time lapse phase contrast and quantitative polarized light microscopy imply that MT polymerization within the bundles provides the compressional

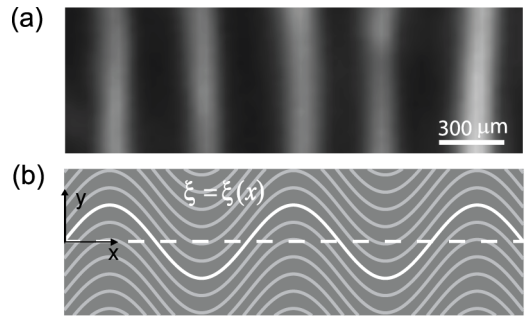


FIG. 1: Image of a MT birefringent pattern and a sketch of the mechanical buckling model. (a) Striped birefringent pattern [23]. The image was taken between crossed polarizers with the polarization directions at  $45^\circ$  with respect to the  $x$  axis. (b) Schematic drawing of buckled MT bundles surrounded by an elastic MT network (gray background). The white dashed line depicts the central bundle before buckling. The white sinusoidal curve depicts the elongated bundle after buckling and the gray sinusoidal curves represent the neighboring MT bundles.  $\xi(x)$  is the transverse displacement for the central bundle.

force. Specifically, they reveal that the bundles elongate uniformly along their contours while maintaining constant radii consistent with growth through the elongation of the individual MTs comprising them. We make predictions for the characteristic buckling wavelength using the bundle bending rigidity and the critical buckling force estimated from the measured MT force-velocity curve. The measured wavelength of about  $600 \mu\text{m}$  implies that the bundles bend as solid rods.

We envision initially the microtubule solution to consist of an array of straight and parallel bundles aligned along the  $x$  axis and embedded in a network composed of dispersed MTs as in Fig. 1(b). All of the bundles experience a similar compressional force that grows to a critical value, causing them to buckle. To describe the buckling, we consider a single bundle in the center of the sample and characterize its interaction with the network using a single elastic constant,  $\alpha$ , such that  $\alpha\xi(x)$  is the elastic restoring force exerted by the network on the bundle per unit length. Treating the bundle as a rod with a bending rigidity,  $K$ , under a uniform compressional force,  $F$ , the force balance in the  $y$  direction at the onset of the buckling

is given by [12, 13, 14]

$$K \frac{\partial^4 \xi(x)}{\partial x^4} + \frac{\partial}{\partial x} \left[ F \frac{\partial \xi(x)}{\partial x} \right] + \alpha \xi(x) = 0 \quad (1)$$

Performing a standard normal mode stability analysis of Eq. (1) using  $\xi(x) \propto e^{ikx}$  yields a relation between the angular wavenumber,  $k$ , and the compressional force,  $F = \alpha/k^2 + Kk^2$ , which suggests a minimum or critical compressional force  $F_c$  for a buckling solution. The critical compressional force is  $F_c = 2\sqrt{K\alpha}$ , and the characteristic wavelength is

$$\lambda_c = 2\pi/k = \pi\sqrt{8K/F_c} = 2\pi\sqrt{K/\alpha} \quad (2)$$

The resultant characteristic wavelength [Eq. (2)] agrees with the prediction for  $\lambda_c$  based on energy minimization [9]. This model predicts buckling in a higher mode than the fundamental one as in classic Euler buckling.

In agreement with experiments, this model implies that the orientation of MT bundles in a striped sample varies continuously in space [9]. In contrast, previous models had suggested that discrete and alternate angular orientations of the MTs formed the striated patterns [15]. In addition, the weak dependence of the buckling wavelength on the mechanical parameters is consistent with the small variations in both the observed buckling wavelength across a single macroscopic sample and the patterns formed under different conditions (for example, samples with different tubulin concentrations and samples in containers with different size.).

Time lapse phase contrast microscopy reveals that the MT bundles elongate uniformly along their contour during buckling, which is consistent with polymerization occurring uniformly along the bundles. The elongation is illustrated in the phase images Fig. 2(a) and Fig. 2(b), showing a fixed region taken 12 and 100 minutes after polymerization initiation, respectively. The three white curves in each image are computer generated traces of bundle contours that extend between selected fiducial marks. The fiducial marks are visible as dark spots in the images. To generate the white curves, we presumed that the bundles followed the striations in the images and traced the stripes between the fiducial marks, whose positions were tracked using the MetaMorph imaging software (Universal Imaging, West Chester, PA). Specifically, we determined the local striation orientation at each pixel by calculating a Fast Fourier Transform (FFT) of the area around the pixel, shown, for example, in Fig. 2(c). The FFT appeared as an elongated spot oriented perpendicular to the striation direction [Fig. 2(d)]. The radially integrated FFT intensity has a peak at a specific azimuthal angle [Fig. 2(d)] that is perpendicular to the striation orientation. In this way, the lengths of three segments along a MT bundle were recorded every 30 seconds and plotted in Fig. 2(f), (g) and (h). The normalized lengths of these three segments grew at nearly the same, constant rate, shown in Fig. 2(i), implying that the MT bundles elongate uniformly along their contour instead of growing

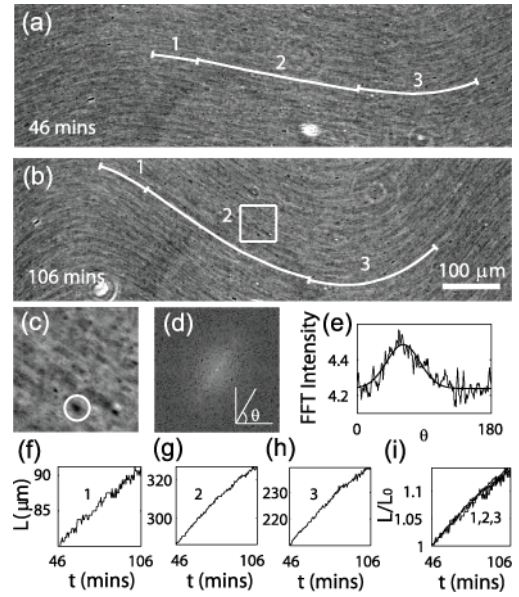


FIG. 2: Illustration and measurements of the uniform elongation of MT bundles [23]. (a,b) Phase contrast images of a sample region, show progression of the pattern over one hour. MT bundles are discerned by the thin striations. The image contrast is enhanced for better visualization. Segments 1 through 3 are adjacent pieces of a contour followed by bundles. The segment ends are defined by fiducial marks. (c) Magnified view of the region denoted by the white box in (b), showing an encircled fiducial mark. (d) Fast Fourier Transform (FFT) of (c). (e) The radially averaged FFT intensity plotted versus the azimuthal angle  $\theta$  and fit using a Gaussian function. The local bundle orientation is orthogonal to the angle at which the Gaussian fit peaks. (f-h) Length of segments 1 (f), 2 (g) and 3 (h) as a function of time. (i) Lengths of the three segments as functions of time, normalized to their lengths at 46 minutes.

solely at their ends. It further suggests that the bundles elongate through polymerization of their constituent MTs, which start and end at random places along a bundle. The uniform growth of all MTs within the bundle justifies a uniform elongation rate and the use of a uniform compressional force throughout the bundle in the mechanical model, giving rise to the sinusoidal  $\xi(x)$  over the entire pattern.

Additional quantitative information about the microscopic picture of the buckling is gained through time-lapse birefringence measurements. PolScope (CRI, Cambridge, MA) images, taken sequentially at a fixed sample region [16], yielded the time evolution at each pixel of both the retardance ( $\Delta \equiv \text{birefringence} \times h$ , where  $h$  is the sample thickness) and the slow axis direction ( $\varphi(x)$ , orientation of MT bundles) [17]. Two representative PolScope images of a single region taken at different stages of self-organization are shown in Fig. 3(a) and 3(b). The slow axis variation,  $\varphi(x)$ , along the white lines in Fig. 3(a) and 3(b) can be fit to  $\varphi(x) = \text{atan}[A \frac{2\pi}{\lambda} \cos(\frac{2\pi}{\lambda}(x+x_0))]$ , indicating that the bundle follows  $\xi(x) = A \sin(\frac{2\pi}{\lambda}(x+x_0))$  with a single wavelength  $\lambda$ , buckling amplitude  $A$ , and offset  $x_0$  [Fig. 3(c)]. The resultant wavelength,  $\lambda \approx 600 \mu\text{m}$ , is plotted in Fig. 3(d). The nor-

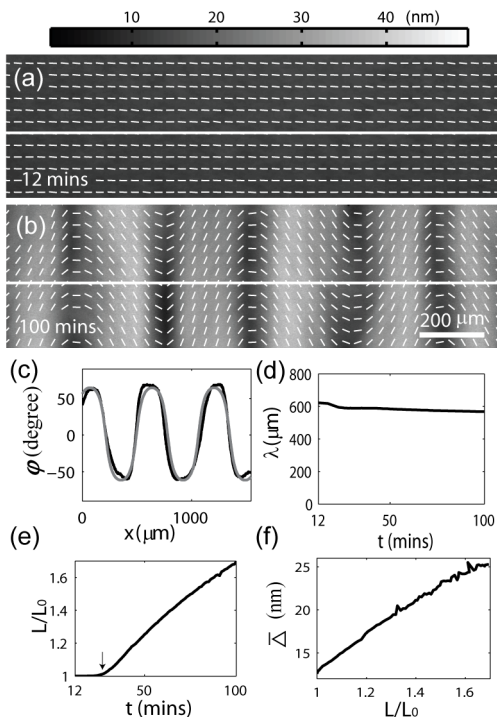


FIG. 3: Time evolution of a MT pattern obtained by measuring the retardance and slow axis of the sample using a PolScope imaging system [16]. (a,b) Retardance images of a sample region at 12 and 100 min of self-organization, respectively. The gray bar shows the retardance magnitude scale and the white pins provide the slow axis orientation. The straight white lines represent the slow axis line scan position. (c) Slow axis line scan (black) and the fitted slow axis orientation  $\varphi(x) = \text{atan}[A \frac{2\pi}{\lambda} \cos(\frac{2\pi}{\lambda}(x+x_0))]$  (gray) at 100 min. (d) The dominant buckling wavelength  $\lambda$ , obtained from the fitted shapes of the bundle at individual time points. (e) The length evolution of the fitted bundle contour.  $L_0 = 1544 \mu\text{m}$  is the initial unbuckled length of the bundle. The segment before the arrow designates a latent period prior to the onset of the buckling. (f) The magnitude of the retardance averaged over the white lines as shown in (a,b) versus the normalized length  $L/L_0$ .

malized contour length calculated from the fits,  $L(t)/L_0$ , grew nearly linearly with time at a normalized rate of  $\dot{L}(t)/L_0 \approx 1\%$  per min [Fig. 3(e)]. Simultaneously, the retardance magnitude averaged over the white line in Fig. 3(a) increased roughly in proportion to  $L(t)/L_0$  [Fig. 3(f)]. Based on the nesting model we proposed earlier and assuming that neighboring MT bundles do not coalesce, the average retardance goes as  $\bar{\Delta}(t) \sim \delta \times n(t)L(t)/L_0$  [9, 17], where  $n(t)$  is the number of MTs in the cross section of a bundle and  $\delta$  is the retardance of a single MT. Therefore, the linear relation between  $\bar{\Delta}(t)$  and  $L(t)/L_0$  implies that  $n(t)$  remains constant throughout buckling. Thus, the elongation of MT bundles occurs through the polymerization of MTs within the bundles and does not involve the incorporation of new MTs to existing bundles.

With the above observations and model, we can quantitatively characterize the elastic properties of the bundle ( $K$ ) and network ( $\alpha$ ). We begin with the implications of the mea-

sured wavelength  $\lambda$ . In order to predict  $\lambda$  from the mechanical buckling model, we need to estimate  $K$  and  $F$  [Eq. (2)]. Two limits exist for  $K$ . If tight packing (solid model) of the MTs inside the bundle is assumed, then  $K_{\text{solid}} = n^2 K_{\text{MT}}$ , where  $K_{\text{MT}} \approx 3.4 \times 10^{-23} \text{N} \cdot \text{m}^2$  is the bending rigidity of a single MT [18, 19]. If MTs slide freely inside the bundle, then  $K_{\text{slip}} = nK_{\text{MT}}$ . We employ the measured force-velocity relation,  $f(v) = C_1 \ln[C_2/(v+C_3)]$  ( $C_1 = 1.89 \text{pN}$ ,  $C_2 = 1.13 \mu\text{m}/\text{min}$  and  $C_3 = -0.08 \mu\text{m}/\text{min}$  [18]), for a single MT and presume  $F = nf(v)$ , where  $v$  is the average elongation rate of individual MT inside the bundle. Writing the average length of MTs inside the bundle as  $l_{\text{MT}}$ , the elongation rate of a single MT is then approximately  $v(l_{\text{MT}}) = l_{\text{MT}} \times \dot{L}(t)/L_0$ . Using the models for  $K$ ,  $F$  and Eq. (2), we derive predictions of  $\lambda$  for both the solid model,  $\lambda_{\text{solid}} = \pi \sqrt{8nK_{\text{MT}}/f(v(l_{\text{MT}}))}$ , and the slip model,  $\lambda_{\text{slip}} = \pi \sqrt{8K_{\text{MT}}/f(v(l_{\text{MT}}))}$ . Each depends on  $l_{\text{MT}}$  and  $n$ . Using  $n = 280$  [9], we plot the wavelength over a reasonable range of individual MT lengths (11) in Fig. 4. The solid model for  $K$  appears much more reasonable than the slip model. The fact that  $K$  depends quadratically on  $n$  in our system suggests that MTs are fully coupled (acting like a solid material) inside the bundle, similar to the behavior of F-actin bundles held together through depletion forces [20]. The bundling of initially aligned MTs can be attributed to the depletion force induced by unpolymerized tubulin dimers, oligomers and even short MTs [9].

The conclusion that the bundles bend as solid rods apparently conflicts with the picture of elongation, that involves the growth and relative sliding of individual MTs within the bundles. We speculate that the explanation involves two distinct time scales: the time for a MT to come to mechanical equilibrium with its neighbors following the insertion of a tubulin dimer to its end,  $\tau_{\text{mech}}$ , and the average interval between insertions,  $\tau_{\text{dimer}}$ . In the limit  $\tau_{\text{mech}} < \tau_{\text{dimer}}$ , strong coupling between the MTs in the bundle can occur leading to the solid rod result. The opposite limit intuitively leads to weak coupling between the MTs within a bundle. We estimate  $\tau_{\text{dimer}} \approx 0.1 \text{s}$  from our data, which seems quite long compared to the times characterizing the relative motion of neighboring MTs on the molecular length scales relevant to  $\tau_{\text{mech}}$ . The exact molecular picture, which goes beyond the scope of our model, needs further study.

Using the solid model for  $K$ , we can calculate the remaining model parameter,  $\alpha$ , from Eq. (2):  $\alpha = K_{\text{slip}}(2\pi/\lambda_{\text{expt}})^4 \approx 0.032 \text{Pa}$ . This value is remarkably small compared to that estimated for a single MT buckling inside a cell ( $\alpha^* \approx 2700 \text{Pa}$  [12]). We identify two contributors to the difference between  $\alpha$  and  $\alpha^*$ . In general,  $\alpha \sim G$ , where  $G$  is the elastic shear modulus of the surrounding network.  $G \sim 1 \text{Pa}$  in our system [21], while  $G^* \sim 1000 \text{Pa}$  for the surrounding cytoskeleton network inside the cell [22]. The other contributor is the coordination of the buckling of the MT bundles, which reduces the distortion of the surrounding network, and thus weakens the effective restoring force and  $\alpha$  (analysis in prepa-

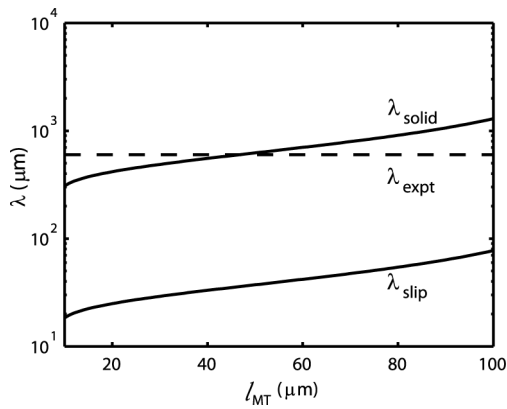


FIG. 4: Theoretically calculated wavelength ( $\lambda$ ) as a function of the average length of MTs ( $l_{MT}$ ) inside the bundle at the onset of buckling. In the solid model  $\lambda_{solid} = \pi\sqrt{8nK_{MT}/f(v(l_{MT}))}$ , and in the slip model  $\lambda_{slip} = \pi\sqrt{8K_{MT}/f(v(l_{MT}))}$ .  $\lambda_{expt}$  is the experimentally observed buckling wavelength (dashed line).

ration).

In summary, using microscopic studies of the temporal evolution of the striated MT patterns, we show that the polymerization of MTs within the bundles causes uniform elongation. This in turn creates the driving compressional force which ultimately causes the MT bundles to buckle. It is this coordinated buckling that produces the striped birefringent pattern. The proposed mechanical buckling model adequately describes the buckling process. It predicts a critical buckling force and a characteristic wavelength, which depend on the elasticity of the surrounding network and the bending rigidity of the MT bundles. Combing the bending rigidity of MT bundles and the established MT force-velocity curve with the mechanical model, we obtain a reasonable estimate for the elastic constant of the network and find that MTs inside the bundle are fully coupled.

We thank Allan Bower for help in understanding the elastic constant  $\alpha$  and thank L. Mahadevan and Thomas R. Powers for valuable discussions. This work was supported by NASA (NNA04CC57G, NAG3-2882) and NSF (DMR 0405156, DMR 0605797).

[1] A. Desai and T. J. Mitchison, *Annu. Rev. Cell Dev. Biol.* **13**, 83 (1997).

[2] D. Bray, *Cell Movement: From Molecules to Motility* (Garland, New York, 2001).

[3] R. P. Elinson and B. Rowing, *Dev. Biol.* **128**, 185 (1988).

[4] G. Callaini, *Development* **107**, 35 (1989).

[5] A. L. Hitt, A. R. Cross, and R. C. Williams, *J. Biol. Chem.* **265**, 1639 (1990).

[6] J. Tabony, *Science* **264**, 245 (1994).

[7] F. J. Nédélec, T. Surrey, A. C. Maggs, and S. Leibler, *Nature* **389**, 305 (1997).

[8] C. E. Walczak, I. Vernos, T. J. Mitchison, E. Karsenti, and R. Heald, *Current Biology* **8**, 903 (1998).

[9] Y. Liu, Y. Guo, J. M. Valles, and J. Tang, *Proc. Natl. Acad. Sci. U.S.A.* **103**, 10654 (2006).

[10] W. Bras, G. P. Diakun, J. F. Díaz, G. Maret, H. Kramer, J. Bordas, and F. J. Medrano, *Biophys. J.* **74** (1998).

[11] N. Glade and J. Tabony, *Biophys. Chem.* **115**, 29 (2005).

[12] C. P. Brangwynne, F. C. MacKintosh, S. Kumar, N. A. Geisse, J. Talbot, L. Mahadevan, K. K. Parker, D. E. Ingber, and D. A. Weitz, *J. Cell Biol.* **173**, 733 (2006).

[13] J. R. Gladden, N. Z. Handzy, A. Belmonte, and E. Villermaux, *Phys. Rev. Lett.* **94**, 035503 (2005).

[14] L. D. Landau and E. M. Lifshitz, *Theory of Elasticity* (Oxford, New York, 1986), 3rd ed.

[15] J. Tabony and N. Glade, *Langmuir* **18**, 7196 (2002); C. Pape-seit, L. Vuillard, and J. Tabony, *Biophys. Chem.* **79**, 33 (1999); J. Tuszynski, M. V. Sataric, and *et al.*, *Physics Letters A* **340**, 175 (2005).

[16] The sample was polymerized from a 5 mg/ml tubulin solution (2 mM GTP, 3.5% in molar ratio of Oregon Green conjugated taxol to tubulin dimers, 100 mM pipes, 1 mM EGTA, 2 mM  $MgSO_4$ , PH 6.9) in a  $40 \times 8 \times 0.4 \text{ mm}^3$  glass cuvette which was exposed to 9 T vertical static magnetic field for 5 minutes at  $37^\circ\text{C}$  (the magnetic field direction is along the long axis of the cuvette). The cuvette was then laid flat on the microscope stage and a coherently buckled area was chosen for observation and measurement at  $30^\circ\text{C}$ .

[17] R. Oldenbourg, E. D. Salmon, and P. T. Tran, *Biophys. J.* **74**, 645 (1998).

[18] M. Dogterom and B. Yurke, *Science* **278**, 856 (1997).

[19] J. A. Tuszynski, T. Luchko, S. Portet, and J. M. Dixon, *Eur. Phys. J. E* **17**, 29 (2005).

[20] M. M. A. E. Claessens, M. Bathe, E. Frey, and A. R. Bausch, *Nature Materials* **5**, 748 (2006).

[21] M. Sato, W. H. Schwartz, S. C. Selden, and T. D. Pollard, *J. Cell Biol.* **106**, 1205 (1988).

[22] R. E. Mahaffy, C. K. Shih, F. C. MacKintosh, and J. Käs, *Phys. Rev. Lett.* **85**, 880 (2000).

[23] The sample was polymerized from 8 mg/ml tubulin solution (same buffer condition as in [16]) in a  $40 \times 10 \times 1 \text{ mm}^3$  quartz cuvette and was subjected to convective flow (induced by asymmetrical thermal contacts, with the left and bottom surfaces in contact with a  $37^\circ\text{C}$  waterbath-warmed aluminum holder and other sides exposed to  $30^\circ\text{C}$  ambient) for the first 9 minutes. The cuvette was then laid flat on the microscope stage for observation and measurement at  $30^\circ\text{C}$ .